Surface Flux Limited Diffusion of Solvent into Polymer

P. J. McDonald,* J. Godward, R. Sackin, and R. P. Sear

Department of Physics, University of Surrey, Guildford, Surrey, GU2 7XH, United Kingdom

Received July 7, 2000; Revised Manuscript Received November 20, 2000

ABSTRACT: Two limiting regimes of small molecule diffusion in polymers are widely acknowledged: Fickian and case II. Case II diffusion is associated with solvent uptake proceeding linearly with time. Linear uptake is normally described by models that assume the viscoelastic polymer swelling at the solvent front to be the rate-limiting step in the transport process. In this paper we observe that, so long as a solvent-driven glass to rubber transition exists, the rate-limiting step can alternately be the solvent flux at the polymer surface. The case II velocity then depends on the surface flux. Varying this flux can vary the case II front velocity in a manner not explicable using established models. It can also drive a transition between Fickian and case II transport. An additional outcome is that varying the solvent flux permits a new method of accessing any concentration history dependence of the solvent diffusivity in the polymer. Numerical simulations of a simple phenomenological model illustrating Fickian diffusion, conventional solvent-front-limited case II diffusion, and surface-flux-limited case II diffusion are presented. The modeling is supported by experimental measurements of liquid and vapor toluene ingress into polystyrene using magnetic resonance imaging (MRI) and stray field imaging (STRAFI). Vapor flux and temperature are varied.

Introduction

The ingress of solvents into polymers is a much studied problem due to its importance to technologies as diverse as food production and civil engineering. However, it remains poorly understood. It is often observed that solvent ingress does not proceed as the square root of time as one might expect from Fickian diffusion. Rather case II ingress is observed.[1] Case II ingress is characterized by a sharp solvent front which ingresses linearly with time into the polymer. Behind the front, the solvent fraction is usually uniform. A Fickian precursor extending a short distance ahead of the front is seen in experiments with sufficient spatial resolution.[2] In 1982, Thomas and Windle[3] proposed the first of a series of models[4,5] which satisfactorily explain most of the observed behavior. These models start from the premise that the polymer is initially glassy. A critical concentration of solvent is required to induce a glass-to-rubber transition. Diffusion of the solvent ahead of the point where its concentration is high enough that the polymer is a rubber is very slow. In the rubber it is rapid. This creates the sharp solvent front. The solvent concentration varies slowly with position up to the front and is close to the equilibrium value for the swollen rubber. The rate-limiting process to solvent ingress is the viscoelastic swelling response of the polymer to the solvent in the glass. This limits the maximum solvent flux at the front. The solvent front advances into the polymer with a constant profile. Consequently, the intrinsic speed of this advance is independent of time, and the front advances linearly. Whenever the rate of advance of the solvent is limited by the rate of advance of a time-independent solvent front, the solvent ingress will be case II. This is case II diffusion as conventionally understood. In light of the work presented in this paper, we term case II diffusion of this kind solvent-front-limited case II diffusion.

If the rate of advance is limited by diffusion from the surface of the swelling polymer to the solvent front, then the ingress will be Fickian. An increase in the speed of swelling at the solvent front relative to the diffusion flux at the front causes a transition from case II to Fickian diffusion with ingress proportional to the square root of time and smooth solvent concentration profiles. In experiment, this transition can be hard to observe as systems are either strongly case II or strongly Fickian. The transition region is often called anomalous diffusion and is said to be exemplified by diffusion proceeding as t^n, where t is time and $0.5 < n < 1$. This crossover is not a true power law however. Three means to accomplish the transition from case II to Fickian can be envisaged. The first is that any case II diffusion process becomes Fickian in the long time limit for very large samples. The flux decreases with increasing distance between the sample surface and the case II front since it is proportional to the solvent gradient between the two. For large enough distances, the diffusive flux becomes smaller than the maximum flux at the solvent front into the glassy polymer, a property of the polymer and solvent system set by the rate at which solvent can drive the initially glassy polymer to the rubber state. We believe that there is no unambiguous observation of the transition occasioned this way. The second means is to vary temperature and thereby hope to increase the maximum flux at the solvent front more quickly than the liquid diffusivity in the rubber. This was explored by some of the current authors in a study of methanol ingress into poly(methyl methacrylate).[6] Finally, it is possible either to vary the composition of the solvent by using mixtures of good and poor solvent or to slightly preswell the polymer with a good solvent before exposing it to a poor solvent.[6]

The purpose of this paper is to point out that there are other circumstances in which a linear advance of the solvent front is found, just as in case II diffusion, but in which the swelling at the solvent front is *not* limiting the speed of ingress. Rather, the speed of solvent ingress is limited by the flux of solvent impinging on the surface of the polymer. We term this surface-flux-limited case II diffusion. This will be observed when the flux of solvent on the surface is reduced. If the surface flux is constant and rate limiting, then the

10.1021/ma001177g CCC: $20.00
Published on Web 00/00/0000 PAGE EST: 9.1

solvent front still advances linearly. However, it does so because the flux of solvent at the solvent front, where the glass-to-rubber transition occurs, is restricted to that at the surface. The reduced flux most readily comes about as a consequence of the solvent being provided in vapor form. We suggest that this is able to account for several otherwise unexplained experimental observations. The two most important of these are (i) some combinations of polymer and solvent such as polystyrene and toluene can exhibit both case II and Fickian behavior and (ii) nuclear magnetic resonance (NMR) measurements in particular sometimes show the dynamics of the rubber changing on time scales orders of magnitude greater than any commonly accepted polymer chain disentanglement time. We use toluene ingress into polystyrene as an example of observation i. The ingress of toluene vapor with low activity was investigated as a case II system by forward recoil ion-beam spectrometry by Gall and Kramer[7] from the viewpoint of exploring the induction period and the early stages of case II front advance. Our own NMR microscopy studies reported below show liquid toluene ingress to be Fickian. Here we explore the situation more carefully. In other work using iodohexane and polystyrene, Hui et al.[8] found a very rapid rise in the case II front velocity at higher equilibrium solvent concentrations which they were unable to explain in terms of the Thomas and Windle model. As an example of observation ii, we cite acetone vapor ingress into poly(vinyl chloride) (PVC), another case II system.[9] This was studied using stray field imaging (STRAFI) and indeed was the first quantitative use in any field of this method. The measurements revealed that the dynamics of the rubber region behind the liquid front were evolving over a period of days.

Here new theoretical insights are supported by NMR microscopy measurements of toluene ingress into polystyrene. NMR microscopy has been widely used previously for studies of this kind by numerous authors.[10−14]

2. The Model

We wish to model the ingress of solvent into a glassy polymer using a simple, minimal model that incorporates only the basics of the physics, the physics which determine the qualitative behavior. The model is phenomenological. If the polymer is uniform parallel to the surface in contact with the solvent, then the solvent advance is one-dimensional. The solvent concentration (number per unit volume), c, depends just on z and t, where z is the distance from the surface of the sample polymer, i.e., $z = 0$ at the surface, and t is the time since the start of polymer ingress into the sample. For convenience, we define a dimensionless concentration $\phi = c/c_m$, where c_m is the maximum concentration of the solvent in the swollen polymer.

2.1. Fickian Diffusion. Let us first consider a very simple system where we just have diffusion into the polymer with a constant diffusion constant D, and the surface is kept at a constant concentration equal to the maximum concentration c_m. Then the evolution of the reduced concentration at a point z and time t is governed by the diffusion equation

$$\frac{\partial\phi(z,t)}{\partial t} = D\,\frac{\partial^2\phi(z,t)}{\partial z^2} \tag{1}$$

subject to the boundary conditions

$$\phi(z>0,t=0) = 0 \tag{2}$$

$$\phi(z=0,t) = 1 \tag{3}$$

The initial condition, eq 2, is that the solvent concentration is zero inside the sample. At the surface, the concentration is at its maximum value c_m and so $\phi = 1$. In eqs 1−3 we neglect the complicating transformation of coordinates necessitated by the sample swelling. Equation 1 with these initial and boundary conditions can be solved analytically,[15] and the result is a solvent front which advances with time as $t^{1/2}$.

Diffusion can be simulated using a cellular-automaton-like system: a system of discrete elements whose time evolution is governed by simple deterministic equations. Space is discretized into elements each of width a along the z direction, and time is discretized into steps of length δt. The reduced solvent concentration in the ith element at time t is denoted by $\phi(i,t)$. Element 1 is the surface element, and analogously to the boundary condition of eq 3 we fix its concentration,

$$\phi(1,t) = 1 \tag{4}$$

In addition the initial condition of eq 2 becomes

$$\phi(i>1,t=0) = 0 \tag{5}$$

The time evolution of the concentrations of the other elements is governed by the equation

$$\phi(i,t+\delta t) = \phi(i,t) + \frac{D\delta t}{a^2}[\phi(i-1,t) - 2\phi(i,t) + \phi(i+1,t)] \qquad i > 1 \tag{6}$$

Our elements are very similar to cellular automata, but the state of a cellular automaton is generally a discrete variable whereas the reduced density $\phi(i,t)$ of our elements is a continuous variable. Using eqs 4−6, we obtain results indistinguishable from those of eqs 1−3, providing our reduced time increment $D\delta t/a^2$ is small and we look at length scales much larger than a.

2.2. Case II. We are interested in solvent advancing into a polymer that is initially glassy. Ingress into a glassy polymer is slow until the solvent concentration is sufficiently high that the glassy polymer becomes a rubber. This limits the flux from the rubber region into the glass. As this can be rate limiting, we must incorporate it into the model.

The solvent front lies at the interface between the glassy and rubbery polymer. We define it to lie between the i_s and $(i_s + 1)$th elements. The distance from the surface is $z_s = i_s a$. For the case of very slow mechanical relaxation of the glassy polymer at the solvent front, the flux of solvent at this boundary is limited. To keep the model as simple as possible, both conceptually and in terms of the number of its parameters, we characterize the glass−rubber boundary with only two parameters. One is the critical reduced concentration of solvent required to transform the polymer glass to a rubber, denoted by ϕ_{rg}. The other is the maximum flux at the solvent front, j_{rg}. As ϕ_{rg} is the concentration at the solvent front, we have that $\phi(i_s,t) \geq \phi_{rg}$, $\phi(i_s+1,t) < \phi_{rg}$. At any time t, i_s is defined as being the largest value of i for which $\phi(i,t) > \phi_{rg}$. It is the element furthest from the surface within which the solvent concentration is high enough for the polymer to be in the rubber state. The slow relaxation at the solvent front is then modeled by limiting the flux from the most advanced rubber

element, element i_s, into the adjacent glassy element, $i_s + 1$. The time evolution of the concentrations in the i_sth and $(i_s + 1)$th elements is governed by the equations

$$\phi(i_s,t+\delta t) = \phi(i_s,t) + \frac{D\delta t}{a^2}[\phi(i_s-1,t) - \phi(i_s,t)] - \frac{j_f\delta t}{c_m a} \quad (7)$$

and

$$\phi(i_s+1,t+\delta t) = \phi(i_s+1,t) + \frac{j_f\delta t}{c_m a} \quad (8)$$

where

$$\frac{j_f\delta t}{c_m a} = \min\left(\frac{j_{rg}\delta t}{c_m a}, \phi(i_s,t) - \phi_{rg}\right) \quad (9)$$

The flux at the solvent front is j_f, and j_{rg} is a model parameter. The latter is the flux flowing into the glassy polymer if the concentration in the adjacent rubber is high enough and is an upper bound to the flux. If the concentration in the last rubber element is very close to ϕ_{rg}, then the flux is lower than j_{rg}. The flux into the glassy element, $i_s + 1$, then tends toward the flux into the last rubber element, i_s, at the previous time step. The change in ϕ is $j_f/(c_m a)$ because the rate of change in concentration c inside a slice of width a due to a flux j_{rg} equals j_{rg}/a. This is then multiplied by our time step and divided by c_m to get the change in the reduced concentration ϕ in a time δt. Beyond the glassy element in contact with the last rubber element, there is no diffusion and $\phi(i) = 0$. The time evolution in the rubber, $i < i_s$, is given by eq 6. The model cannot predict the Fickian precursor because within it there is no diffusion in the glass.

To summarize, when the polymer sample is in contact with solvent, the boundary and initial conditions are still eqs 4 and 5. Within the rubber region, $i < i_s$, the concentrations still evolve according to eq 6. However, the two elements that form the front, $i = i_s$, $i_s + 1$, evolve according to eqs 7 and 8, and the concentrations in the glassy region, $i > i_s + 1$, are static.

There are two competing rates, the slower of which will be rate limiting. For a solvent front at z_s, one rate, the characteristic speed, comes from diffusion of the solvent from the surface in contact with the solvent, $z = 0$, to the solvent front. This diffusive speed is $s_D = D/z_s$. It can be determined from dimensional analysis or by differentiating the $t^{1/2}$ advance of the diffusion-limited advance of a solvent front. The second characteristic speed of advance is for the glass-to-rubber transition at the solvent front, $s_{rg} = j_{rg}/(c_m\phi_{rg})$.

If $s_D \ll s_{rg}$, i.e., diffusion from the surface to the solvent front is limiting the speed of advance of the solvent front into the polymer, then our results are little different from Fickian diffusion without the boundary condition of eqs 7 and 8. The solvent front advances into the polymer as $t^{1/2}$. However, in the opposite limit, $s_D \gg s_{rg}$, then it is the glass-to-rubber transition at the solvent front itself which is limiting the speed of advance. Then the solvent front advances linearly into the polymer; i.e., it advances as t. This is solvent-front-limited case II ingress. Our model is close to being the simplest possible. As s_D decreases as $1/z_s$ while s_{rg} is fixed, once our model parameters are set, then for sufficiently large z_s, occurring after sufficiently large times, the advance of the solvent front will *always* be diffusion-limited and the front will always advance as $t^{1/2}$. Of course, in experiment this will only be observed if the polymer is thick enough. The crossover will occur at $s_D = s_{rg}$ or $z_s = Dc_m\phi_{rg}/j_{rg}$.

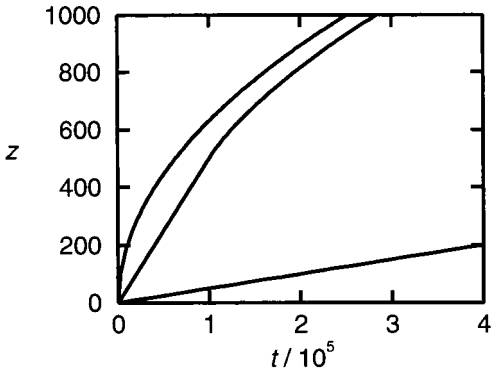

Figure 1. Calculations of the advance of the solvent front. The x axis is time in units of a^2/D; our time step $\delta t = 0.1a^2/D$. The y axis is the position of the solvent front in units of the element width a. From top to bottom, $\alpha = 10^{-2}$, 10^{-3}, and 10^{-4}.

To illustrate the behavior of our model, we have performed some example calculations and plotted the results in Figure 1. There are two dimensionless parameters: ϕ_{rg} and $\alpha = j_{rg}a/(D_{cm})$. The ratio α is equal to s_{rg}/s_D with s_D evaluated at $z_s = a$. We set $\phi_{rg} = 0.2$. This is a reasonable value, and our results are not sensitive to the precise value of ϕ_{rg}. The results are presented with a^2/D as the time unit and a as the length unit. With ϕ_{rg} fixed we have only one parameter left, α. We plot results in Figure 1 for $\alpha = 10^{-2}$, 10^{-3}, and 10^{-4}. For 10^{-2} the solvent advance is close to $t^{1/2}$, whereas for 10^{-4} it is linear for all times shown. The intermediate value of α is linear up to a time of about 10^5 but then curves over and is tending toward a $t^{1/2}$ dependence. This is what we expect, as, for $\alpha = 10^{-3}$ the solvent front should be diffusion-limited for z_s greater than approximately $10^3 a$.

2.3. Low Flux at the Surface. Some experiments are performed with the polymer in contact not with liquid solvent but with solvent vapor. The flux of solvent at the surface of the polymer is much lower when in contact with vapor than when in contact with liquid solvent. It can be so low as to be rate limiting. This is easy to model. We replace the boundary condition of eq 4 with a constant flux, j_v, at the surface,

$$\phi(1,t+\delta t) = \min\left(\phi(1,t) + \frac{D\delta t}{a^2}[\phi(2,t) - \phi(1,t)] + \frac{j_v}{c_m a}, 1\right) \quad (10)$$

i.e., there is a constant flux j_v into the surface unless this flux would cause the concentration to exceed the maximum concentration.

If we compare eqs 7 and 10, we see that they are rather similar; both control the flux at the boundary of the region of rubber polymer. Equation 10 controls the flux into the rubber. Equation 7 controls the flux out of the rubber. Either can be rate limiting. As with the solvent front we can define a characteristic constant speed of advance, now due to the flux at the surface. This speed of advance is $s_v = j_v/(c_m\phi_{rg})$. It is the rate at which the solvent front advances if the flux at the surface is the limiting factor, rather than the flux at the solvent front or diffusion from the surface to the

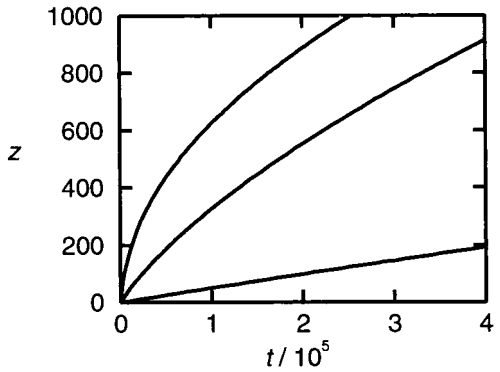

Figure 2. Calculations of the advance of the solvent front. The x axis is time in units of a^2/D; our time step $\delta t = 0.1a^2/D$. The y axis is the position of the solvent front in units of the element width a. From top to bottom, $\beta = 10^{-2}$, 10^{-3}, and 10^{-4}; $\alpha = 10^{-2}$.

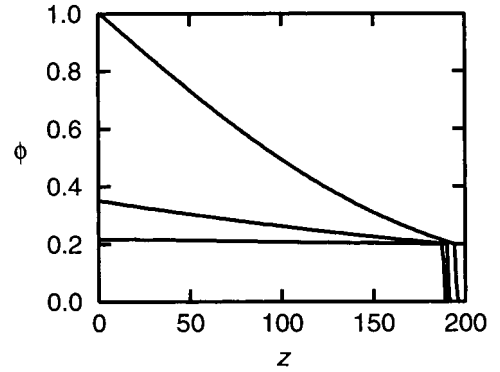

Figure 3. Three solvent profiles, ϕ as a function of z, are plotted. They are plotted at different times, each when the front has moved a distance close to $200a$. From top to bottom the curves are for $\beta = 10^{-2}$, 10^{-3}, and 10^{-4}, respectively; $\alpha = 10^{-2}$. The three curves are at times 12 000, 51 000, and 390 000, in units of a^2/D, for $\beta = 10^{-2}$, 10^{-3}, and 10^{-4}, respectively. The time step $\delta t = 0.1a^2/D$.

solvent front. It will be rate limiting when $s_v \ll s_D$, s_{rg}. Linear ingress occurs even if $s_{rg} \gg s_D$. Hence, a linear advance is seen for a polymer and solvent combination which is Fickian when the polymer is in contact with the liquid solvent. We call this solvent-front-limited case II diffusion.

To illustrate the behavior of our model, we have performed some example calculations and plotted the results in Figure 2. The model has three dimensionless parameters: ϕ_{rg} and the ratios $\alpha = j_{rg}a/(Dc_m)$ and $\beta = j_v a/(Dc_m)$. Once these are fixed, we can use eqs 6−8 and 10 to obtain the position of the solvent front and the concentration profile of the solvent at any time. $\phi_{rg} = 0.2$ as before. If s_v is much larger than the other two, we are back to the situation just considered. So, we consider only $s_v \leq s_{rg}$. Results are presented in Figure 2 for $\alpha = 10^{-2}$ and $\beta = 10^{-2}$, 10^{-3}, and 10^{-4}. For $\beta = 10^{-4}$ the solvent front advances linearly. For $\beta = 10^{-2}$ it advances as $t^{1/2}$. For $\beta = 10^{-3}$ it is never a straight line although it is also not a simple $t^{1/2}$ either: over the range plotted in Figure 2 neither diffusion nor flux at the surface is completely dominant. Solvent profiles at approximately the same position are plotted in Figure 3. When the ingress is limited by the flux at the surface, the solvent concentration profile is rather flat and the concentration is everywhere near ϕ_{rg}. Because the solvent front is advancing as fast as solvent arrives at the surface, the solvent concentration does not build up as it does when the ingress is Fickian or solvent-front-limited case II. Hence, although both solvent-front-limited case II and surface-flux-limited case II ingress result in a solvent front advancing linearly with time, the solvent concentration profiles are very different. In the latter case the concentration behind the solvent front is only a little above that of the rubber−glass transition while for the former it can be much higher. In both cases the concentration profile will be close to a straight line as in both cases diffusion is a fast process relative to the advance of the solvent front.

2.4. Relation to Previous Work. It is interesting to relate the phenomenological model just described to more detailed analyses to be found in the literature.[3−5] Whereas we start by simply setting the flux into the glassy polymer to be very small, previous authors have used models in which viscoelastic relaxation couples to the diffusion of the solvent. Essentially, solvent diffuses very slowly into the glassy polymer which then swells very slowly to accommodate more solvent; as it does so the diffusion coefficient rapidly increases. This slow diffusion into the glassy polymer and the subsequent swelling of the polymer, which both occur at the solvent front, then limits the speed of ingress. If, following Lasky et al.,[16] we neglect the rapid variation of the viscosity as solvent diffuses into the polymer and consider some effective viscosity of the glass η_g, then swelling takes a time of order $\eta_g/(ckT)$, where ckT is an approximation to the osmotic pressure exerted by the solvent. Similarly, we neglect the rapid variation of the diffusion constant in the glassy polymer and consider some effective diffusion constant, D_g. Then the width of the solvent front is the distance the solvent diffuses in a time $\eta_g/(ckT)$, which is $[D_g\eta_g/(ckT)]^{1/2}$. An estimate of the velocity of advance of the solvent front, our s_{rg}, is then $[D_g ckT/\eta_g]^{1/2}$.[16] So, our s_{rg} parameter can be estimated if the time taken for the initially glassy polymer to swell and the distance the solvent diffuses in this time are both known.

3. Determining the Diffusion Coefficient When the Front Velocity Is Constant

Fick's law states that the flux $j(z,t)$ is proportional to the concentration gradient, so that

$$D(z,t) = -\frac{j(z,t)}{\partial c(z,t)/\partial z} \tag{11}$$

where the diffusion coefficient, D, is considered a function of concentration history and hence position and time. If we know both the flux of ϕ and the concentration gradient at a point in space and time, we can obtain the diffusion coefficient. If the solvent profile is unchanging with time except for a steady advance at a velocity v, then the flux at each point is simply the concentration at that point multiplied by the velocity

$$j(z,t) = vc(z,t) \tag{12}$$

Using this equation to substitute for j in eq 11, we have

$$D(z,t) = -\frac{vc(z,t)}{\partial c(z,t)/\partial z} \tag{13}$$

If, in an experiment, we can determine c and its derivative with respect to position, then, for a solvent front advancing at a constant known velocity v, we can determine the diffusion coefficient. In the context of the current work, where we are able to vary the velocity by

varying the incident flux, this offers a means of determining the diffusion coefficient in nonequilibrium situations. In particular, where D is history-dependent, we can use eq 13 to obtain values of D and, at least in principle, study the history dependence by varying v.

4. Experimental Methods

Both liquid-state magnetic resonance microscopy (MRM)[17] and broad line stray field imaging (STRAFI)[18,19] have been used to investigate the absorption of toluene into polystyrene. Toluene of HPLC grade was obtained from Sigma Aldrich (UK). The polystyrene of molecular weight $M_w = 696\,500$ and polydispersity 1.05 (for STRAFI) or $M_w = 1.46 \times 10^6$ and polydispersity 1.04 (for MRM) was obtained as a powder from Polymer Laboratories (UK). It was pressed at 50 kN m^{-2} into small cylindrical pellets at 180 °C for 8 h and slowly cooled to room temperature all under vacuum. The pellets were 8 mm in diameter and 4 mm long. The pellets were pushed into close-fitting cylindrical poly(tetrafluoroethylene) sleeves open at one end. The use of these sleeves ensured that the solvent ingress was unidirectional. This was confirmed by two-dimensional MRM measurements. For MRM measurements, the sleeved pellets were immersed in liquid toluene within the imaging magnet. The volume of liquid far exceeded that of polymer, so that it could be considered an infinite reservoir. For MRM measurements, a standard two-dimensional Fourier transform imaging sequence was used with the following experimental parameters: echo time, 14.5 ms; maximum phase gradient and read gradient strengths, 2.45 and 9.79 G/cm, respectively; and repetition time, 1 s. The chosen slice width was typically 1 or 2 mm, and 512 and 128 read points and phase encode steps were used. After standard Fourier data processing, the resulting in-plane image pixel size was 23 μm by 94 μm and the true resolution somewhat less. MRM images visualized the swollen polymer and solvent solution. The signal intensity was, however, attenuated by nuclear spin relaxation and self-diffusion as is always the case with such imaging. Nonetheless, a distinct rubber/glass interface could be resolved. To achieve more quantitative composition data, stray field profiles were also collected. Stray field imaging uses a much larger gradient strength, here 5800 G/cm, and a much shorter first echo time, here 70 μs. This dramatically alleviates the signal attenuation problem, and as many echoes can be collected in a train, it is possible to visualize the solvent, the swollen polymer, and (strongly attenuated even at 70 μs) the glassy polymer components. By fitting two component decays to the data sets in the rubber region, it is possible to extract the solvent fraction. The disadvantage is that the necessarily increased bandwidth of the method reduces the signal-to-noise ratio of the profile data.

For vapor ingress experiments, a reservoir of toluene was held close to the sample, within the glass tube. For most experiments, the reservoir was above the sample so that the exposed sample surface was uppermost. This arrangement was preferred as it prevented gravitational flow of the swelling sample. Figure 4 shows a schematic of the sample cell arrangement. The vapor path length, d, and the vapor cross section to the sample surface, a, were controlled so that the flux could be evaluated. The path length and cross section were adjusted by varying the glass rod between the sample and liquid reservoir. An additional glass rod was used above the reservoir to fill unwanted space so that the vapor pressure would build rapidly. The critical vapor path is shown unshaded in the figure. This arrangement was used for path lengths, d, of 3.5, 9.5, and 19.5 cm with $a = 0.13$ cm^2. A shorter path length of 0.3 cm was obtained in one experiment by suspending an inverted sample directly over the bath.

As well as extensive measurements at magnet bore temperature (17 °C), measurements for one vapor path length were also made as a function of temperature. In this case a Chemagnetics heater stack operating with temperature controlled air flow was used. The temperature in the sample environment was independently calibrated using a PT 100 resistor. The temperature was controlled to ±0.1 °C.

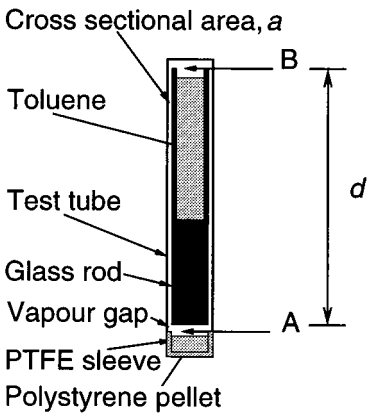

Figure 4. Schematic diagram of the sample cell used for the majority of the vapor ingress stray field profiling experiments. Glass is shown solid black and the vapor space unshaded. The polystyrene sample is at the bottom in a PTFE sleeve. The liquid toluene reservoir is at the top. The vapor path length d and the annular path cross section a are indicated.

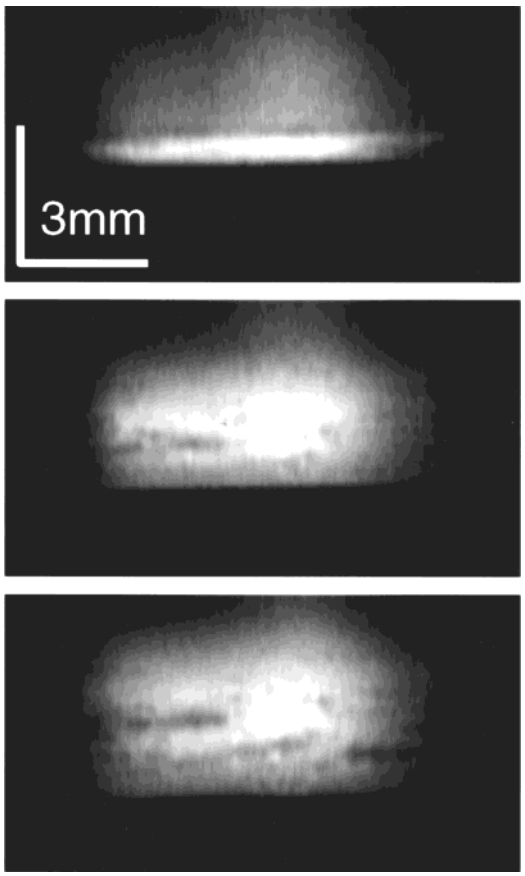

Figure 5. A series of three magnetic resonance images of liquid toluene ingress into polystyrene. The images are recorded after 0.3, 2.3, and 4.3 h. The glassy polystyrene occupies the dark region at the base of each image. The swollen polymer and solution appear bright. The progression of the solvent front into the glass is well delineated.

5. Results and Analysis

5.1. MRM of Liquid Ingress. Figure 5 shows three typical MRM images of liquid toluene ingress into polystyrene; these are recorded at approximately 2 h intervals. The toluene rapidly swells and dissolves the polymer. The top part of each image shows the (diffusion attenuated) solution merging into the rubber. This interface is not well resolved for the experimental parameters used. The rubber appears somewhat brighter,

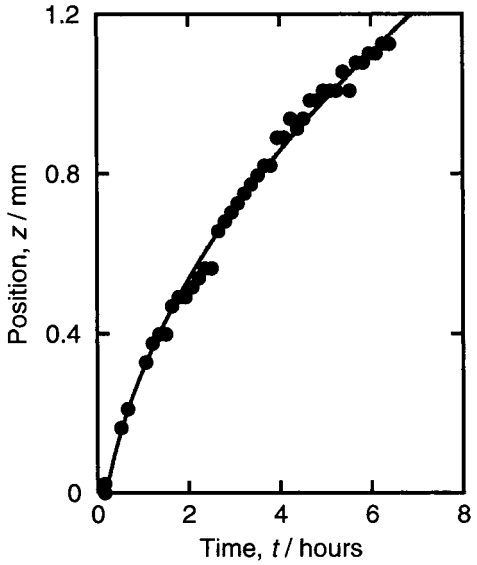

Figure 6. Position of the solvent front relative to the original sample surface for liquid toluene ingress into polystyrene as a function of time. The solid line is a fit to the equation $z = At^{1/2} + z_0$.

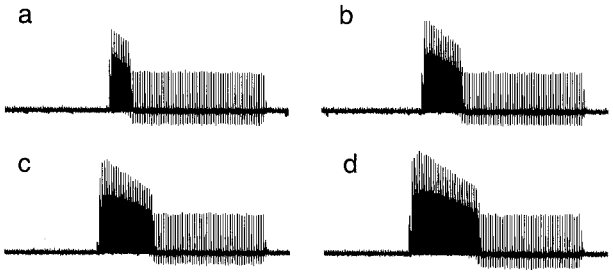

Figure 7. Raw data stray field profiles of the ingress of toluene vapor (d = 3.5 cm) into polystyrene at 17 °C. The profiles are recorded after (a) 30, (b) 60, (c) 90, and (d) 120 h. The profiles consist of 128 magnetic resonance spin-echo trains. Each train consists of 16 echoes recorded over 1120 μs. The trains are recorded at different slices of the sample separated by 60 μm. Hence, each profile is 7.68 mm long. To the left of each profile is the vapor space (no signal) and to the right the glassy polymer (strongly attenuated signal). The rubber is between. Within the rubber, the echo trains are biexponential decays. Even by eye, it is possible to estimate the solvent fraction.

and the sharp interface with the polystyrene glass is well delineated. The glass itself appears dark. Figure 6 shows the absolute (relative to laboratory coordinates) position of the rubber glass interface as a function of time. The solid line shows the result of fitting the data to the equation $z = At^{1/2} + z_0$. Hence, it is shown that the front position varies with the square root of time, characteristic of Fickian diffusion. The small offset z_0 allows for difficulty in determining the time zero interface position. From the fit to the data, it is possible to extract a characteristic diffusivity. The diffusivity measured this way is 9.1×10^{-7} cm^2 s^{-1}.

5.2. Stray Field Profiling of Vapor Ingress. Contrasting behavior is observed if toluene vapor is used in place of toluene liquid. Figure 7 shows a typical set of STRAFI profiles for toluene vapor ingress into polystyrene. In this case, the vapor path is 3.5 cm. The source reservoir is pure liquid toluene. The profiles comprise the MR spin-echo train recorded at each sample location. The profiles shown were recorded at intervals of 30 h. To the left of each profile is the vapor space and to the right the glassy polymer showing as a

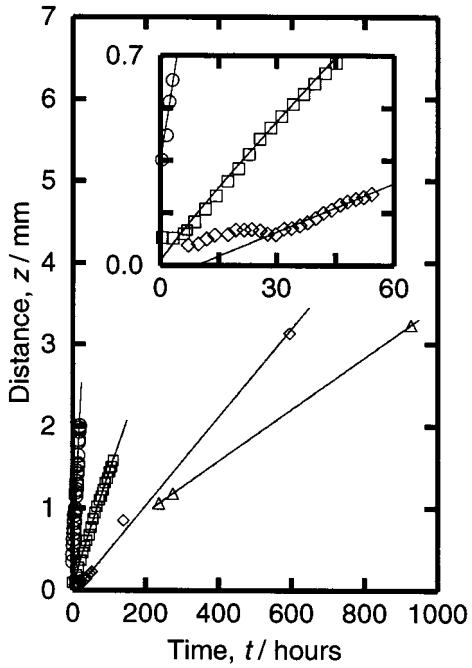

Figure 8. Width, z, of the swollen polymer region for vapor toluene ingress into polystyrene at 17 °C as a function of time, t. Data are shown for path lengths, d, of 0.3 (circles), 3.5 (squares), 9.5 (diamonds), and 19.5 cm (triangles). The solid lines are straight line fits to the data. The inset shows the early development.

series of short decay trains. The central region of larger amplitude decays is the rubber. The sample surface and rubber interface are well-resolved. In the rubber, each echo train comprises a two-component decay: one for the polymer and one for the solvent. The component fractions can be separated by the numerical fitting of biexponential decays to the echo train data at each location after the usual rescaling of the first echo to correct for systematic low intensity.[20] In practice, to achieve this fitting, the longer time component is represented by a constant baseline.

Figure 8 shows the position of the absorption front as a function of time for this sample. After an initial period during which the surface concentration apparently builds up, a sharp solvent front ingresses linearly with time into the sample. This is surface-flux-limited case II diffusion and contrasts strongly with the Fickian diffusion for liquid ingress discussed in the previous section. The initial period should not be confused with the induction period often reported for case II systems.[7] The solvent front observed by MRI is broadened by the point spread function of the profile resolution. In consequence, in the early stages, while the distance ingressed is less than the profile resolution, the intensity within the first few pixels is seen to rise, but the profile width does not increase appreciably. Figure 8 also shows data for the other three path lengths. The front velocities are 24.4, 5.1, 1.6, and 0.9 nm s^{-1} for path lengths of 0.3, 3.5, 9.5, and 19.5 cm, respectively. This compares with a front velocity of 0.04 nm s^{-1} at 20 °C in an ion beam experiment reported by Gall and Kramer[7] for deuterated toluene vapor into polystyrene. This sample was exposed to a very low vapor activity toluene/polystyrene solution but at an unspecified vapor path length. It is instructive to correlate the observed front velocity with the incident vapor flux. The vapor flux arriving at the sample surface is evaluated using Fick's first law. The calculation requires knowledge of

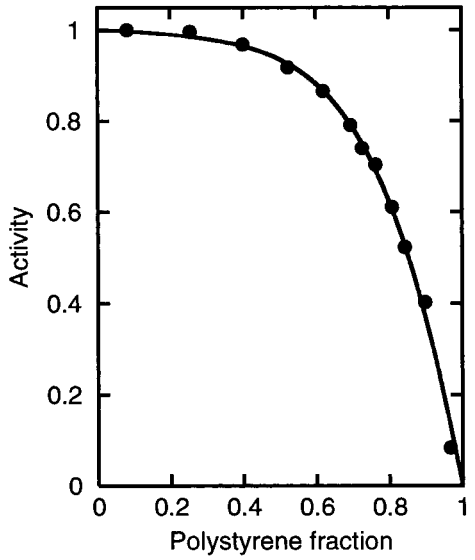

Figure 9. Activity of toluene vapor above polystyrene/toluene solutions as a function of polystyrene fraction. The data are reproduced from Bawn et al.;[22] the solid line is a fit to Flory–Huggins theory.[23]

vapor concentrations above the reservoir and sample (at points A and B in Figure 4, respectively) and of the vapor diffusivity, which is assumed constant. Literature values were used for the vapor concentration above the reservoir.[21] At 17 °C it is close to 3000 N m^{-2}. The vapor pressure above the sample surface was evaluated from literature values for the activity of toluene above polystyrene/toluene mixtures[22] and calculations of the surface toluene fraction from NMR data. The activity data are reproduced in Figure 9 along with a fit to it according to Flory–Huggins theory.[23] The constant vapor diffusivity, D_v, was calculated using ideal gas kinetics[24] according to

$$D_v = \frac{3}{8}\left(\frac{\pi}{2}\right)^{1/2}\frac{1}{c_{air}\sigma^2}\left(\frac{RT}{M}\right)^{1/2} \qquad (14)$$

where R is the universal gas constant, T is temperature, $M = M_T M_A/(M_T + M_A)$ is the reduced molecular weight of toluene molecules in air, M_T is the molecular weight of toluene, M_A is the effective molecular weight of air, c_{air} is the number density of air molecules, and σ is the effective molecular diameter. Assuming $M = 11.08$g, $c_{air} = 2.49 \times 10^{24}$ m^{-3} and $\sigma = 3.36 \times 10^{-10}$ m, then D_v ranges from 1.75×10^{-5} m^2 s^{-1} at 17.0 °C to 1.99×10^{-5} m^2 s^{-1} at 100.9 °C.

The STRAFI data can be used to estimate the sample surface solvent fraction from which the vapor pressure immediately above the surface can be calculated. The sample surface toluene fraction can be estimated either from the amplitudes of two-component fits to the profile data in the surface region or, if it is assumed that the concentration is uniform, by combining knowledge of the overall sample volume increase and the size of the rubber region. In practice, the two methods give results comparable within ±0.05. For the $d = 3.5$ cm data, the surface solvent fraction is approximately 0.35.

The vapor pressures c_A^{vap} and c_B^{vap} and diffusivity D_v so evaluated are combined to give the vapor flux according to $j_v = D_v(c_A^{vap} - c_B^{vap})/d$. Figure 10 shows that there is a good correlation between the flux arriving at the sample surface and the front velocity. This is despite the considerable errors involved in estimating both the swelling and the incident flux. That the correlation exists over 2 orders of magnitude well demonstrates how case II diffusion can be surface-flux-limited.

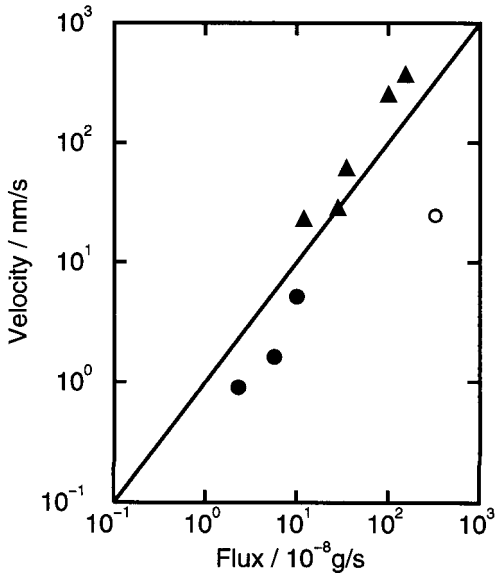

Figure 10. Case II front velocity as a function of toluene vapor flux at the polystyrene surface. The circles are for variable path length data at 17 °C. The open circle is for the inverted sample where sample flow was a problem. The triangles are for $d = 3.5$ cm data at various temperatures. For high-temperature data, where there is deviation from case II ingress, the velocity in the early stages of ingress is used.

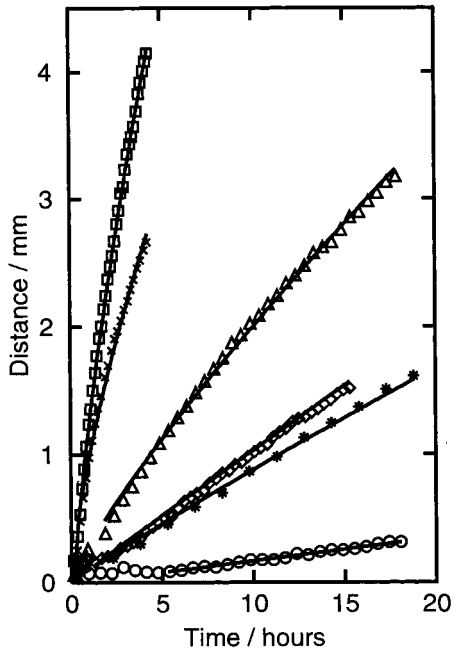

Figure 11. Width, z of the swollen region for toluene vapor ingress into polystyrene as a function of time for $d = 3.5$ cm. The data are recorded at 17 (circles), 41.5 (stars), 47.8 (diamonds), 73.3 (triangles), 85.6 (crosses), and 100.9 °C (squares). The solid lines are fits to the equation $z = A\,t^n + z_0$ over the regions indicated.

5.3. Variable Temperature Measurements. Figure 11 summarizes the temperature dependence of toluene vapor uptake for the path length of 3.5 cm in the temperature range 17–101 °C. At higher temperatures there is a noticeable transition away from linear ingress toward ingress proceeding as $t^{1/2}$. The data have been

Table 1. Calculated Parameters for Surface-Flux-Limited Diffusion of Toluene Vapor into Polystyrene for the Experimental Temperatures Used

temp/°C	vapor press./N m^{-2}	$D_v/10^{-5}$ m^2 s^{-1}	solvent flux/10^{-8} g s^{-1}	n
17.0	3 000	1.75	10	1.06
41.5	9 160	1.83	12	0.93
47.8	11 700	1.84	28	0.98
73.3	36 000	1.92	35	0.83
85.6	49 100	1.95	100	0.72
100.9	79 100	1.99	125	0.72

fitted to the expression $z = At^n + z_0$ where the offset allows for difficulty in accurately locating the sample surface, especially at higher temperatures where the ingress speed requires much more rapid data acquisition with a commensurate reduction in the signal-to-noise ratio. The fits are shown as solid lines in the figure, and the exponent fit parameter, n, is given in Table 1. In this temperature range, according to ideal gas kinetics, the vapor diffusivity increases by 14%. However, the vapor pressure above the reservoir increases dramatically (Table 1). The overall result is a substantial increase in the flux of solvent arriving at the sample surface. The procedure of fitting a single power law follows common precedent. Ideally, given the thrust of this work, one would have preferred to fit two power laws, t^1 and $t^{1/2}$, in the early and later stages of ingress, respectively. However, the volume of data available is insufficient to do this satisfactorily.

If it is assumed that, at sufficiently short times, the ingress is surface-flux-limited, then again a correlation can be made between the flux arriving and the early front velocity. This correlation is made in Figure 10 where it is seen that the variable temperature data broadly reproduce the variable path data. At higher temperatures, with increased surface flux (and also diffusivity in the polymer), this linear ingress breaks down, equivalent to an increase of the parameter β in the model. The correlation is also degraded by the fact that the effective surface concentration varies with temperature as the case II behavior breaks down. Consequently, the coefficient of proportionality between the flux and velocity is not constant with temperature.

5.4. Determination of Toluene Diffusivity in Polystyrene. Figure 12 shows three typical solvent fronts for data recorded for vapor ingress at 17 °C with $d = 3.5$ cm. They are displaced so that the solvent fronts coincide at $z' = z - vt = 0$. After an initial period during which the front shape is forming, profile (a), the profiles overlay each other profiles (b) and (c). By drawing a tangent to the profiles at any given concentration, it is possible to evaluate the diffusivity using eq 13. The diffusivity thus obtained relates to the time since the profile front first passed, $-z'/v$. In general, it is expected that the diffusivity depends not merely on the concentration but also on the concentration history. When the profiles overlay, we can use eq 13 to calculate D as a function of concentration for the particular concentration history of that experiment. A tangent is drawn in the figure for the overlaying profiles at $\phi = 0.225$. Using eq 13, the nonequilibrium diffusion coefficient is calculated as 5.7×10^{-8} cm^2 s^{-1}. This compares with values of 6.8×10^{-8} and 5.8×10^{-8} cm^2 s^{-1} for the same concentration for data recorded with vapor path lengths of 9.5 and 19.5 cm, respectively, showing good agreement between the data sets. The values compare well with literature values for similar systems.[6,14]

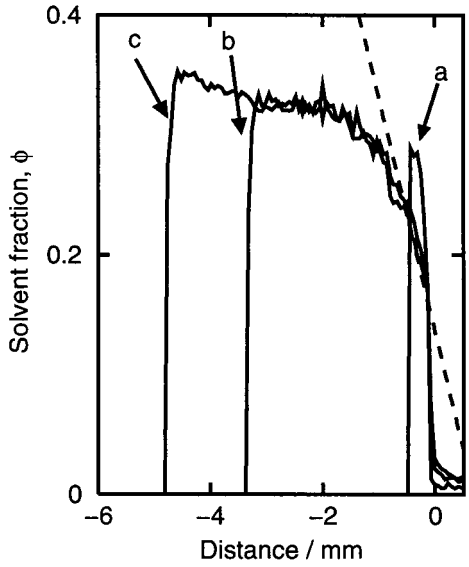

Figure 12. Three solvent fraction profiles extracted from STRAFI toluene vapor ingress data with $d = 3.5$ cm at 17 °C, recorded after (a) 17 h, (b) 8 days, and (c) 13 days. The profiles have been shifted so that the solvent front positions are at $z' = 0$. After an initial development stage, the front shape assumes a constant, pseudo-equilibrium, form. The dashed line is a tangent to this shape from which the diffusivity at $\phi = 0.225$ is calculated.

In principle, diffusivities can be evaluated for earlier profiles such as profile (a) in Figure 12 if the flux is determined from the time dependence of the profile shape. From this analysis, estimates of the concentration history dependence of the diffusion coefficient might be made for various $c(t)$. However, it would appear that the spatial and temporal resolution of MR are inadequate to really study the very earliest profile shapes, so that true temporal dependence cannot be obtained. An additional problem with the MR data is the unambiguous separation of the solvent and polymer. At high solvent fractions, the solvent diffusivity decreases the apparent spin relaxation time of the solvent in the magnetic field gradient, and at the same time the spin relaxation time of the polymer increases. Separation based on two-component exponential fitting then becomes very difficult. Nonetheless, this analysis points the way to future studies where alternate data, such as are obtained from ion beam analysis, might be used for such purposes. The specific advantage of using different vapor path lengths is that they trace alternate cuts through the $D(c,t)$ space.

At low solvent concentrations, the sample is glassy. The same method of evaluating the diffusion coefficient can be used in principle, but now the gradient is so steep as to be limited by the pixel resolution and only an upper bound on the diffusivity can be obtained. Moreover, it is not clear that Fick's first law remains valid and that higher-order terms need not be included.

Finally, Figure 13 shows the equilibrium D at a concentration of 0.3 as a function of temperature obtained from the combined data sets. For this purpose, at higher temperatures only the early, more linear, parts of the ingress data have been used. If it is assumed that the diffusivity in the rubber obeys an Arrhenius relationship, then the inferred activation energy for the more secure lower temperature data, where pixel resolution is not a limiting factor, is 22 kJ mol^{-1}. This value

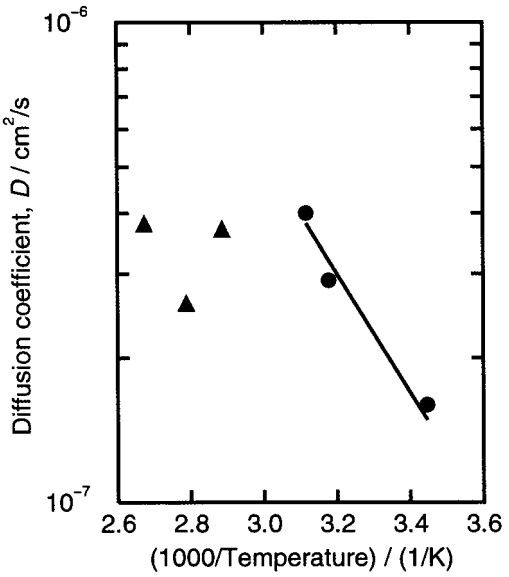

Figure 13. Pseudo-equilibrium toluene diffusion coefficient, D, in polystyrene at $\phi = 0.3$ as a function of temperature. The triangles are high-temperature data where it is believed that the solvent concentration gradient, from which the diffusion coefficient is evaluated, is pixel-resolution-limited. The solid line assumes an Arrhenius behavior with an activation energy of 22 kJ mol^{-1}.

is comparable with other reported values for small molecule diffusion processes in polymers.[6,7,12,16,25]

6. Discussion

The results of the current work explain a number of puzzles originating from earlier work. In particular, a plausible explanation emerges as to why, in experiments looking at acetone vapor ingress into PVC, the polymer chain dynamics were observed to evolve across the rubber region. This equated to evolution for long periods (days).[9] With limited solvent flux at the sample surface, the solvent concentration in the polymer is near uniform and is close to that corresponding to the glass−rubber transition rather than the (much higher) equilibrium concentration. The (very) small concentration gradient close to the transition is sufficient to give rise to large changes in polymer mobility. It also becomes possible to explain the unusually large extent of the Fickian precursor ahead of the main solvent front seen in the same experiments. In the model as described in this paper, the solvent diffusivity in the glass is set to zero. In reality, it will be very small, but nonzero. With low vapor flux, the Fickian precursor has time to build. The new results explain why some systems can be both Fickian and case II. The observed diffusion depends on experimental conditions and not on the viscoelastic properties of the polymer. For solvent-flux-limited case II diffusion, the case II velocity depends solely on the solvent flux at the surface. It is possible, too, that the current work explains why the ion beam data of Hui et al.[8] on iodohexane ingress into polystyrene led these authors to infer solvent diffusivities in the glassy state which apparently varied between samples. The experiment involved exposing glassy polymer to vapor above equilibrated iodohexane/polystyrene solutions. The front velocity increased markedly with the solvent fraction in the reservoir. It is now apparent that the variable in this work was the vapor flux to which the samples were exposed.

In this paper, we have demonstrated both by simple numerical modeling and by experiment that limiting the flux of a solvent impinging on a glassy polymer sample can result in case II diffusion of the solvent into the polymer. This contrasts with case II diffusion as normally described, where the rate-limiting step is the swelling of the polymer at the solvent front.

It has been shown that, by varying the solvent flux, it is possible to vary the case II front velocity. It is worth emphasizing that the low surface flux is necessary but not sufficient to cause case II ingress of this kind. A low flux of diffusant applied to a matrix will normally result in Fickian transport. The special boundary condition of the glass-to-rubber transition remains necessary for linear ingress. Without it, even if the diffusion coefficient is a strong function of concentration, the flux at the solvent front is always proportional to the concentration gradient and generalized Fickian diffusion must result, with D a function of c. It is also worth emphasizing that case II diffusion is a transitory phenomena. Left long enough in a sufficiently large system, the diffusion will always revert to Fickian behavior. It has been shown that the solvent diffusion coefficient can be derived readily from the solvent concentration profile when the incident solvent flux is limited. It is suggested that, with higher temporal and spatial resolution data, this provides a means of readily accessing the concentration history dependence of the diffusivity—if such history dependence exists—in the region of the solvent-induced glass transition.

Acknowledgment. The authors thank Dr. J. L. Keddie (University of Surrey) for useful discussions. This work is funded by the UK Engineering and Physical Sciences Research Council (Grant GR/M 00268). R.S. acknowledges a research studentship from the same Council.

References and Notes

(1) Alfrey, T. *Chem. Eng. News* **1965**, *43*, 64.
(2) Mills, P. J.; Palmstrom, C. J.; Kramer, E. J. *J. Mater. Sci.* **1986**, *21*, 1479.
(3) Thomas, N. L.; Windle, A. H. *Polymer* **1982**, *23*, 529.
(4) Gao, P.; Mackley, M. R. *Proc. R. Soc. London A* **1994**, *444*, 267.
(5) Wu, J. C.; Peppas, N. A. *J. Appl. Polym. Sci.* **1993**, *49*, 1845.
(6) Lane, D. M.; McDonald, P. J. In *Spatially Resolved Magnetic Resonance*; Blumler, P., Blumich, B., Botto, R., Fukushima, E., Eds.; Wiley-VCH: Weinheim, Germany, 1998.
(7) Gall, T. P.; Kramer, E. J. *Polymer* **1991**, *32*, 265.
(8) Hui, C. Y.; Wu, K. C.; Lasky, R. C.; Kramer, E. J. *J. Appl. Phys.* **1987**, *61*, 5137.
(9) Perry, K. L.; McDonald, P. J.; Randall, E. W.; Zick, K. *Polymer* **1994**, *35*, 2744.
(10) Mansfield, P.; Bowtell, R.; Blackband, S. *J. Magn. Reson.* **1992**, *99*, 507.
(11) Hyde, T. M.; Gladden, L. F.; Mackley, M. R.; Gao, P. *J. Polym Sci., Polym. Chem.* **1995**, *33*, 1795.
(12) Ercken, M.; Adriaensens, P.; Reggers, G.; Carleer, R.; Vanderzande, D.; Gelan, J. *Macromolecules* **1996**, *29*, 5671.
(13) Ghi, P. Y.; Hill, D. J. T.; Maillet, D.; Whittaker, A. K. *Polymer* **1997**, *38*, 3985.
(14) Weisenberger, L. A.; Koenig, J. L. *Macromolecules* **1990**, *23*, 2445.
(15) Crank, J. *The Mathematics of Diffusion*; Oxford University Press: Oxford, UK, 1975.
(16) Lasky, R. C.; Kramer, E. J.; Hui, C. Y. *Polymer* **1988**, *29*, 1131.
(17) Callaghan, P. *Principles of Nuclear Magnetic Resonance Microscopy*; Oxford University Press: Oxford, UK, 1991.
(18) Samoilenko, A. A.; Artemov, D. Y.; Sibel'dina, A. L. *JETP Lett.* **1988**, *47*, 348.
(19) McDonald, P. J.; Newling, B. *Rep. Prog. Phys.* **1998**, *61*, 1441.

(20) Benson, T. B.; McDonald, P. J. *J. Magn. Reson.* **1995**, *A112*, 17.
(21) Weast, R. C. *Handbook of Chemistry and Physics*; CRC Press: Cleveland, OH, 1974.
(22) Bawn, C. E. H.; Freeman, R. F. J.; Kamaliddin, A. R. *Trans. Faraday Soc.* **1950**, *46*, 677.
(23) Flory, P. J. *Principles of Polymer Chemistry*; Cornell University Press: Ithaca, NY, 1953.
(24) Kennard, E. H. *Kinetic Theory of Gases*; McGraw-Hill Book Company: New York, 1938.
(25) Lee, P. I. *Polymer* **1993**, *34*, 2397.
MA001177G